CHAPTER FOUR

Mechanisms of Preservation of the Eccentricity and Longer-term Milankovitch Cycles in Detrital Supply and Carbonate Production in Hemipelagic Marl-Limestone Alternations

Mathieu Martinez
Univ Rennes, CNRS, Géosciences Rennes, Rennes, France
E-mail: mathieu.martinez@univ-rennes1.fr

Contents

Abstract

Eccentricity cycles often exert a strong influence on sedimentary series, while they only have weak powers in the insolation series. Three case studies previously published in Early Cretaceous hemipelagic marl-limestone alternations of the Tethyan area are reviewed here to evaluate possible mechanisms of transfer of power from the precession to the eccentricity band. In all cases, the sedimentation rates vary cyclically, following the 405-kyr and the 2.4-myr eccentricity cycles. Maximums of sedimentation rates occur in more clayey intervals, suggesting a strong eccentricity forcing on detrital supply and consequently on sedimentation rates. In all sections, proxies related to purely detrital input show an overwhelming influence of the 405-kyr and the 2.4-myr eccentricity cycle compared to the other Milankovitch components. Proxies related

Stratigraphy & Timescales, Volume 3
ISSN 2468-5178
https://doi.org/10.1016/bs.sats.2018.08.002

to the carbonate production show lower amplitudes of the 405-kyr cycle and enhanced 100-kyr eccentricity cycle, which can dominate the power in the Milankovitch band.

Memory effects of erosional and pedogenetic processes are proposed as powerful mechanisms of transfer of amplitude from the precession to the eccentricity band. Highly evolved pedogenesis under more humid climates have longer memory effects, which favor the 405-kyr and the 2.4-myr cycles in sedimentary series. Changes in phasing between carbonate production and insolation can suppress the low frequencies and favor the dominance of the 100-kyr eccentricity cycle. Consequently, in Tethyan Early Cretaceous deposits, clay-dominated marl-limestone alternations are associated to higher sedimentation rates and higher amplitudes of the long eccentricity cycles. Conversely, carbonate-dominated marl-limestone alternations are associated to lower sedimentation rates and higher amplitudes of the 100-kyr eccentricity cycles.

1. INTRODUCTION

Hemipelagic marl-limestone alternations of the peri-Tethyan area constitute spectacular testimonies of the orbital imprint on sedimentation during the Early Cretaceous (Fig. 1). The analysis of the clay mineralogy (Cotillon, 1987; Cotillon et al., 1980; Deconinck and Chamley, 1983), of the palynofacies (Kujau et al., 2013), the radiolarian assemblages (Darmedru et al., 1982; De Wever, 1987), the calcareous nannofossil and foraminiferal assemblages (Giraud et al., 2013; Mutterlose and Ruffell, 1999) all show a cyclic behavior following the marl-limestone alternations and allowing the discard of an early diagenetic origin of these alternations. The analysis of clay mineral assemblages between marl and limestone beds has been particularly crucial to validate the hypothesis of an orbital origin (Westphal et al., 2010). In sections having experienced low levels of burial (Deconinck and Debrabant, 1985), marl beds are enriched in kaolinite and illite, while limestone beds are enriched in smectite (Fig. 2). Enrichment in kaolinite and illite indicate high levels of continental weathering and runoff, at the origin of a high-level hydrolysis, erosion of soils and detrital input to the basin (Deconinck and Chamley, 1983; Moiroud et al., 2012; Mutterlose and Ruffell, 1999). Conversely, enrichment of smectite in limestone beds indicate low levels of continental weathering and runoff leading to lower detrital input to the basin under semi-arid conditions. Cycles in palynofacies assemblages also indicate higher humidity levels in marly intervals than in calcareous intervals, in agreement with the clay mineral assemblages (Charbonnier et al., 2016; Kujau et al., 2013). Neritic and pelagic floro-faunal communities respond to these changes in climate and detrital supply.

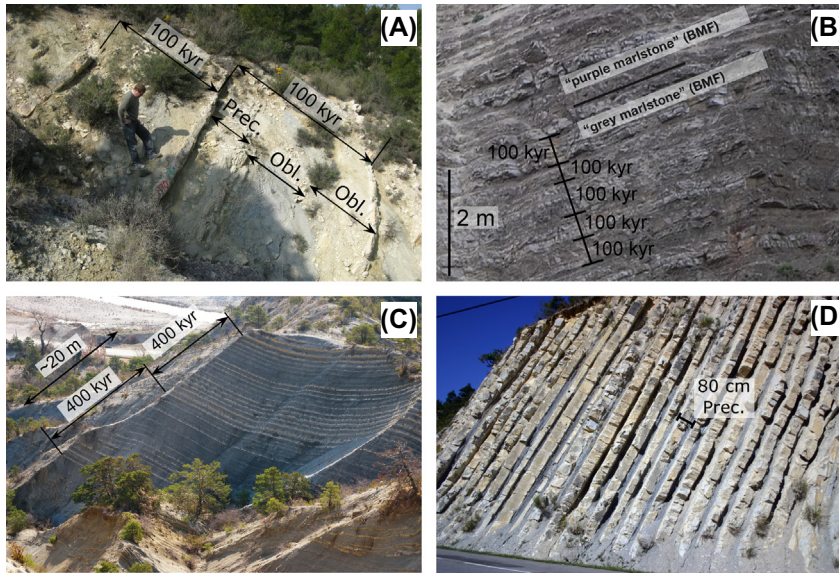

Figure 1 Four examples of marl-limestone alternations in the case studies introduced in this paper. (A) Bundles of 100-kyr eccentricity in the Río Argos section (SE Spain, Hauterivian-Barremian boundary). (B) Bundles of 100-kyr eccentricity in the Bersek Quarry (Hungary, uppermost Valanginian). (C) Bundles of 405-kyr eccentricity in the La Charce section (SE France, Upper Valanginian). (D) Marl-limestone alternations in the La Charce section (Lower Hauterivian). Abbreviations: *Obl.*, Obliquity; *Prec.*, Precession.

In pelagic environments, mesotrophic communities are found in marl intervals while oligotrophic communities are observed in limestone beds suggesting a strong positive coupling of the detrital and the nutrient input to the basin (Giraud et al., 2013; Mutterlose and Ruffell, 1999). Interestingly, the flux of nannofossils is more important in marl beds than in limestone beds, suggesting that nannoplankton productivity was higher during deposition of the marls (Gréselle et al., 2011), while exports from carbonate platforms to the basin led to the deposit of limestone beds in hemipelagic settings (Colombié and Strasser, 2003; Pittet, 2006; Pittet and Mattioli, 2002; Schlager et al., 1994).

Analyses of the stacking and of the frequency content of the marl-limestone alternations commonly evidence the influence of orbital forcing, which controlled the sea-level and climatic changes at the origin of the lithologic alternation (Gilbert, 1895; Giraud et al., 1995; Hinnov and Park, 1999; Moiroud et al., 2012; Pittet and Mattioli, 2002). Spectral analyses of sedimentary series evidence a strong direct control of the eccentricity

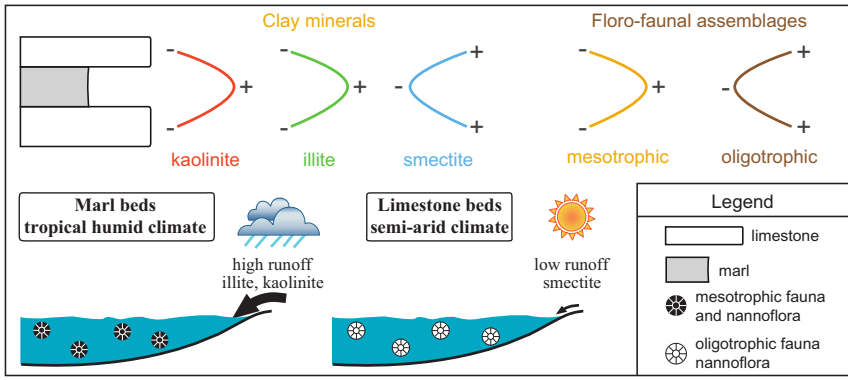

Figure 2 Model of orbital forcing on humid–arid cycles, marl-limestone alternations, clay minerals and floro-faunal assemblages. *Modified from Mutterlose, J., Ruffell, A., 1999. Milankovitch-scale palaeoclimate changes in pale–dark bedding rhythms from the Early Cretaceous (Hauterivian and Barremian) of eastern England and northern Germany. Palaeogr. Palaeocl. 154, 133–160.*

cycles to the deposit of the marl-limestone alternations (Fig. 1), while the power of the eccentricity cycles is nearly null in the insolation cycles. This has arisen the question of the mechanisms of transfer of power from the precession to the eccentricity cycles in the absence of major episode of glaciation during the Cretaceous (Herbert, 1994; Laurin et al., 2015). In these studies, distortion of power, by varying the carbonate production in pelagic environments, and threshold effects at high latitudes have been suggested as mechanisms of transfer from short to long Milankovitch cycles. Surprisingly, while hemipelagic alternating deposits are commonly used to produce orbital time scales (Giraud et al., 1995; Martinez et al., 2017; Meyers and Sageman, 2004), the potential mechanisms of transfer of power from short (precession) to long Milankovitch cycles (eccentricity) in sedimentary basins have not been studied.

In order to highlight such potential mechanisms of power transfer in Early Cretaceous hemipelagic environments, this paper aims at deciphering the impact of the detrital supply and carbonate production on the genesis of the marl-limestone alternations and on the expression of the eccentricity cycles. To address this problem, three case studies are considered: (i) the control of purely detrital proxies vs. mixed carbonate-detrital proxies on the expression of eccentricity cycles at the Hauterivian-Barremian transition of the Subbetic Domain (SE Spain); (ii) the link between detrital supply and bulk carbonate carbon isotopes in the Geresce Mountains (Hungary); (iii) the long-term trend in the detrital supply throughout the

Valanginian-Hauterivian in the Vocontian Basin (South-Eastern France). Through these case-studies, I show that the cycles in detrital supply tend to act as natural low-pass filters, diminishing the amplitude of the precession and obliquity cycles. The phasing between carbonate $\delta^{13}C$ and the lithology can change, likely in function of the balance between the neritic export of carbonate to the basin, the pelagic production and the type of carbonate producers in neritic environments, enhancing the expression of the 100-kyr cycle.

2. GEOLOGICAL SETTINGS

The three cases studies considered here are on Early Cretaceous hemipelagic deposits that were all situated on the Northern margin of the Tethys Ocean (Fig. 3). Their paleolatitude ranged from 20° to 30°N (Dercourt et al., 1993).

The Subbetic Domain is located in the external part of the Betic Range in Southeastern Spain. This hemipelagic domain was separated from the neritic Prebetic Domain during a phase of extensional tectonics during the Early Jurassic, linked to the rifting of the Alpine Tethys (Martín-Algarra

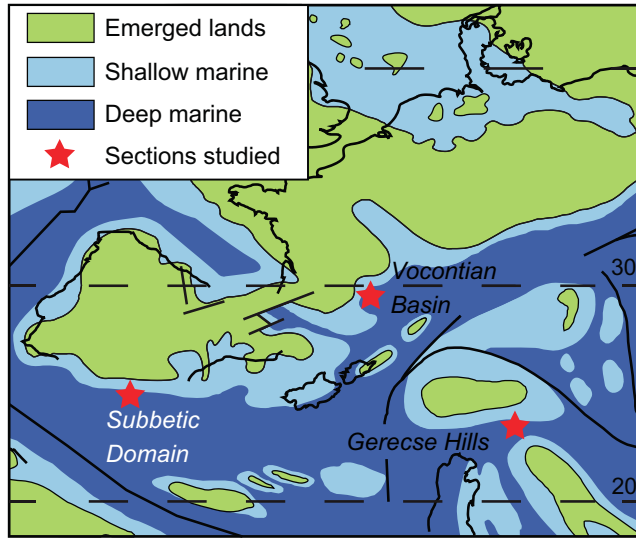

Figure 3 Paleogeographic map of the Western Tethys in the Early Cretaceous with locations of the sections studied. *From Dercourt, J., Ricou, L.E., Vrielynck, B., 1993. Atlas Tethys Paleoenvironmental Maps. Gauthier-Villars, Paris, France.*

et al., 1992; Vera, 2001). During the Early Cretaceous, the Iberian bloc experienced a transtensional motion related to the opening of the North Atlantic and the Alpine oceans (Vera, 2001). The section shown here corresponds to the Hauterivian-Barremian transition of the Río Argos section. The section is composed of marl-limestone alternations deposited in a hemipelagic environment as testified by the numerous ammonites, belemnites, calpionellids and calcareous nannofossils encountered there (Hoedemaeker and Leereveld, 1995). The section has been accurately dated by ammonites and is the current candidate for the Global Stratotype Section and Point (GSSP) of the Barremian Stage (Ogg et al., 2016).

The Vocontian Basin is part of the Dauphinois Zone in the external western Alps. The basin is surrounded by the Provencal carbonate platform to the South, the Ardeche Margin to the West, and the Jura-Dauphiné carbonate platform to the North (Cotillon, 1971). The Vocontian Basin experienced high subsidence rates during the middle Jurassic linked to the rifting phase of the Alpine Tethys (Lemoine et al., 1986; Stampfli and Borel, 2002). The shift from rift to drift tectonics occurred during the Late Jurassic (Roux et al., 1988). Consequently, during the Early Cretaceous, basins in the Northern Tethyan margin experienced decreased subsidence rates (Lemoine et al., 1986; Wilpshaar et al., 1997). The marl-limestone alternations of the Vocontian Basin were deposited in a hemipelagic environment, as evidenced by the ammonites, the belemnites, the calpionellids and the calcareous nannofossils found in this area (Blanc, 1996; Bulot et al., 1993; Thierstein, 1973). Here, I focus on two sections of the basin, the Vergol-Morénas section and the La Charce-Pommerol section (Martinez et al., 2015). Numerous ammonites provided a reference stratigraphic framework in these sections (Bulot et al., 1993; Reboulet and Atrops, 1999) and the sections can be correlated using a series of marker beds as references (Cotillon, 1971; Reboulet and Atrops, 1999). These marker beds form a series of bundles which correspond to the record of the 405-kyr eccentricity cycle (Martinez et al., 2015, Fig. 1). I therefore grouped the two sections as a unique composite series. Detailed bulk carbonate $\delta^{13}C$ curves have been provided in both sections (Gréselle et al., 2011; Hennig et al., 1999; Kujau et al., 2012; van de Schootbrugge et al., 2000), providing a reference curve for stratigraphic correlations (Föllmi, 2012).

The Gerecse Hills are in the NE part of the Transdanubian Mounts, between the Vértes Hills to the South and the Pilis Hills to the East. They are part of the ALCAPA Terrane in the Apulian bloc (Csontos and Vörös, 2004). During the Early Cretaceous, the Gerecse Hills were in the

southern side of a flexural basin delimited to the East and the North by prism wedges related to the subduction of the Vardar Ocean (Fodor and Főzy, 2013). The Gerecse Hills remained nonetheless far from the deformation zones during the Valanginian-Hauterivian times (Fodor et al., 2013). The sedimentation in the eastern Gerecse Hills is composed of mixed marl-limestone alternations, while the western part of the Gerecse is marked by deposits of pelagic limestone until the end of the Valanginian, probably at a higher relief position (Császár and Árgyelán, 1994). The section studied here is an outcrop in the Bersek Quarry in the eastern part of the Gerecse Hills. This outcrop is the type-section for the Bersek marl formation and is composed of 31.2-m thick alternations between marl and mudstone beds, in which cm-thick glauconitic sandstone beds intercalate. The sediments are rich in ammonite and calcareous nannofossils, indicating a hemipelagic environment (Fogarasi, 2001; Főzy and Janssen, 2009). The fossil content and bulk carbonate $\delta^{13}C$ allowed the section to be dated as Late Valanginian, the base of the section starting in the Plateau phase of the Weissert Event (Bajnai et al., 2017).

3. RÍO ARGOS

Clay mineral assemblages, Magnetic Susceptibility (MS) and $\%CaCO_3$ were acquired in the Río Argos section (Martinez et al., 2012; Moiroud et al., 2012, Fig. 4). Clay mineral assemblages are composed of illite, R0-type smectite-illite mixed layers (thereafter assimilated to smectite), kaolinite and chlorite. Illite and smectite compose more than 90% of the clay mineral (Moiroud et al., 2012). Within a marl-limestone alternation, marls are enriched in kaolinite and illite, while limestones are enriched in smectite, as commonly observed in the marl-limestone alternations of the peri-Tethyan area (Fig. 2). Kaolinite is a mineral forming in a context of strong hydrolysis of silicate from the continental crust under tropical, annually humid conditions, while smectite are formed in context of moderate hydrolysis of silicates from the continental crust, under temperate or semi-arid conditions (Chamley, 1989). Illite and chlorite are observed in endogenous rocks, and their export to the sedimentary basins are thus linked to the mechanical erosion of soils. Enrichment of illite and kaolinite together in marls signs a tropical humid climate marked both by strong levels of chemical hydrolysis and continental weathering, while such processes are only moderate during the deposition of the limestone beds. The MS signal shows

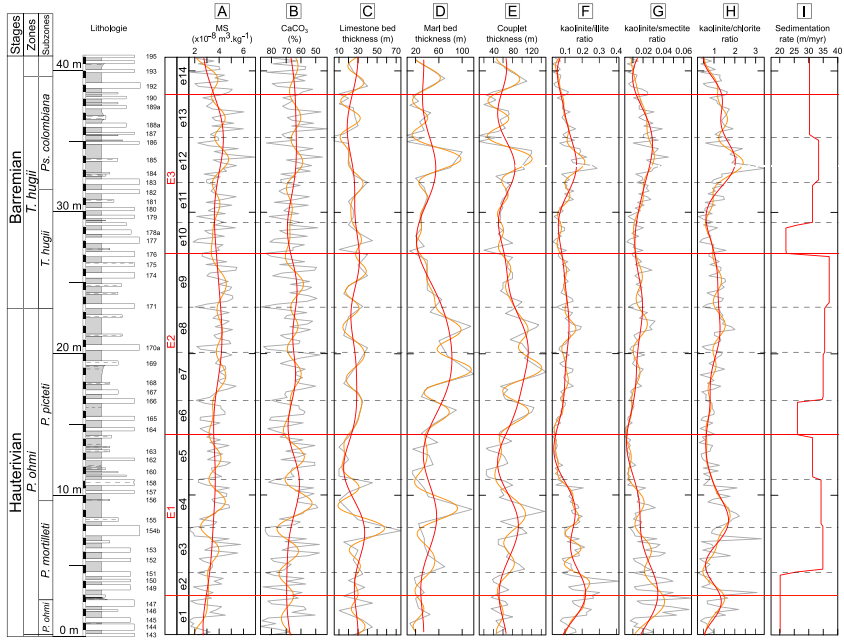

Figure 4 Magnetic susceptibility (MS), $CaCO_3$ content, clay mineral content ratios and bed thicknesses in the Río Argos sections. The original clay mineral assemblages can be found in Moiroud et al. (2012). The *red curves* represent the Taner low-pass filters of the 405-kyr eccentricity band in each proxy while the *orange curves* represent the Taner low-pass filters of the whole eccentricity band (405 + 100-kyr eccentricity) in each proxy.

a strong inverse correlation with $\%CaCO_3$ ($r = -0.94$) and has an intercept MS value of 9.7×10^{-9} m^3/kg when $\%CaCO_3$ is 0 (Fig. 5). This is close to the specific MS value of illite or smectite (Hunt et al., 1995), which are the dominant minerals in the clay assemblages. In other words, the MS signal is essentially controlled by paramagnetic clay minerals, and its fluctuations are controlled by dilution effects of the carbonate content. Clay minerals are thus regarded here as proxies for the fluctuations in the detrital supply while MS and $\%CaCO_3$ are proxies for the change in lithology.

Spectra were generated using the multi-taper method (MTM; Thomson, 1982, 1990) applying three 2π-tapers with confidence levels calculated with the Mann and Lees (1996) method modified in Meyers (2014). The filters were performed using Taner low-pass filters (Taner, 2003). The settings of all filters are indicated in Fig. 5. The interpretations in terms of orbital forcing are from Martinez et al. (2012, 2015) and Moiroud et al. (2012). The 405-kyr eccentricity band has periods ranging

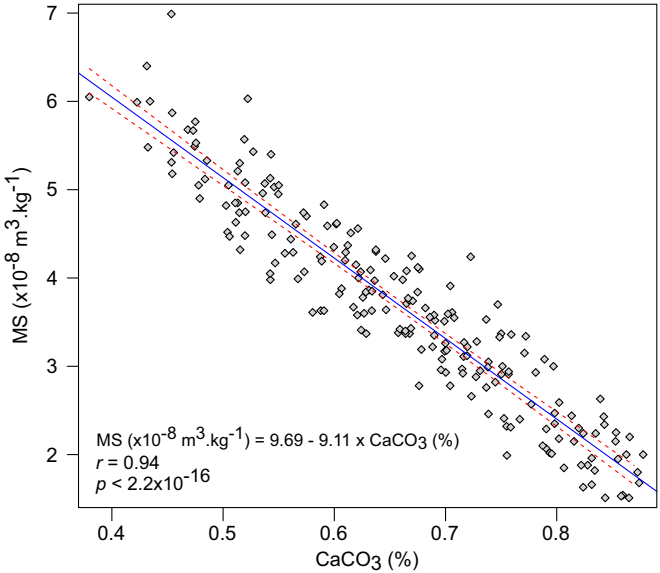

Figure 5 Cross-plot between the magnetic susceptibility (MS) and the $CaCO_3$ content in the Río Argos section. The *blue line* represents the best-fit linear regression while the *red curves* represent the 95% confidence intervals.

from 20 m to 11.8 m (Fig. 6). This large range is due to the intensification of the continental weathering during the Faraoni Oceanic Anoxic Event (Baudin and Riquier, 2014; Moiroud et al., 2012; Sauvage et al., 2013), leading to an increase in kaolinite content in the clay minerals and deviating their period of the 405-kyr to lower frequencies (Martinez et al., 2015). The average period of the 405-kyr eccentricity band without the spectra of the clay minerals is 14.0 m. The 100-kyr eccentricity shows periods ranging from 2.7 to 3.4 m with an average period of 3.2 m. The obliquity has periods ranging from 1.3 to 1.0 m, with an average period of 1.1 m. The precession band show periods ranging from 0.74 to 0.54 m, with an average period of 0.63 m. The spectra of the MS series and $\%CaCO_3$ show higher power in the 100-kyr eccentricity band than in the 405-kyr eccentricity band, while the clay mineral ratios show much higher powers in the 405-kyr eccentricity than in other bands (Fig. 6). This is clearly shown in the filter outputs of the whole eccentricity band in Fig. 4. The filter outputs of the eccentricity band in MS and $\%CaCO_3$ show a higher amplitude at the 100-kyr band while the filter outputs of the eccentricity band in the clay mineral ratios have higher amplitudes in the 405-kyr band.

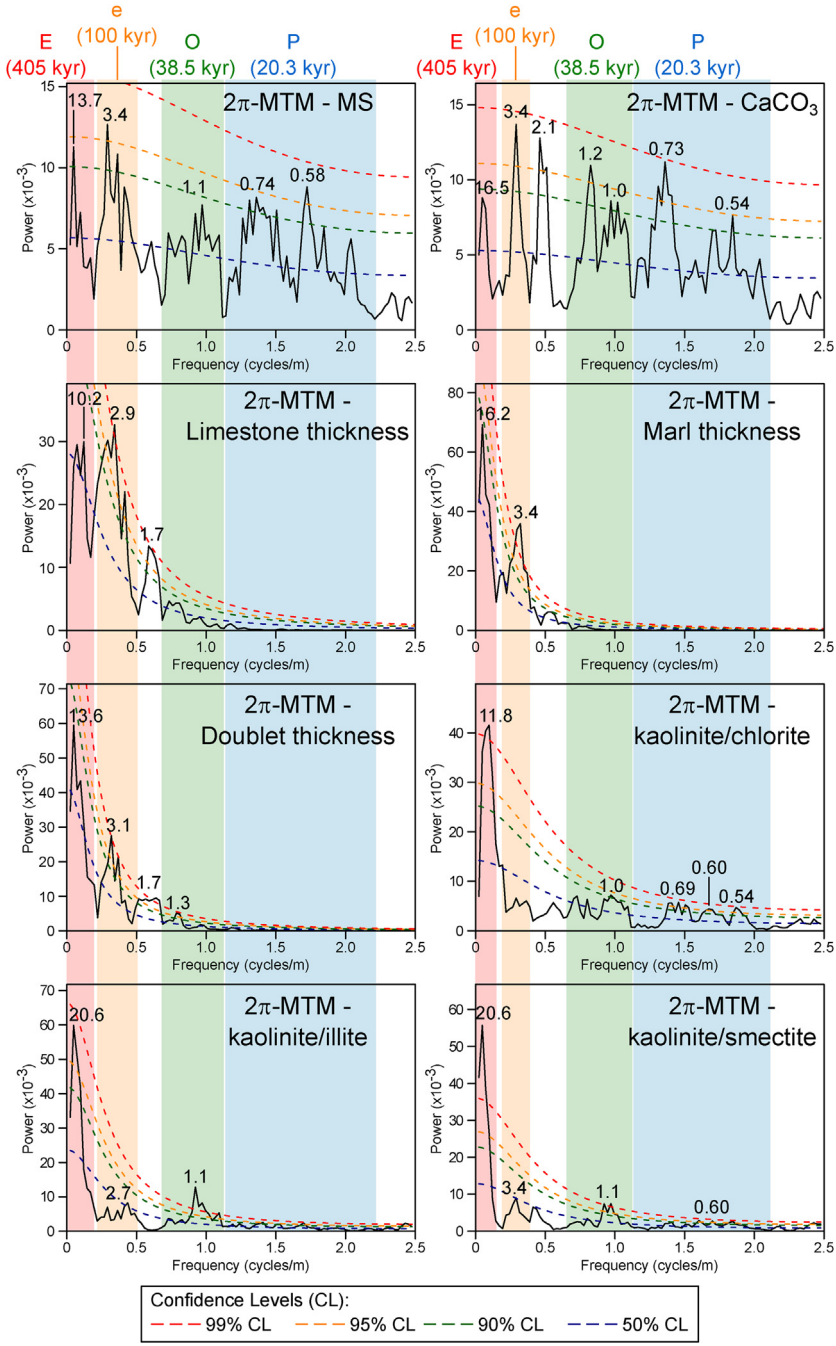

Figure 6 2π-MTM spectra of the proxies shown in Fig. 4.

The orbital tuning of the MS series to the 100-kyr eccentricity shows a cyclicity of 405 kyr, with lower sedimentation rates in calcareous intervals also marked by lower kaolinite/illite, smectite or chlorite ratio (Fig. 4). Higher levels of continental weathering are thus associated to higher detrital supply and higher sedimentation rate. I report here the thicknesses of marl beds, limestone beds, and marl-limestone couplets (Fig. 4) and calculate their 2π-MTM spectra (Fig. 6). The spectra of the marl and marl-limestone couplet thicknesses show a clear dominance of the 405-kyr eccentricity cycle compared to the 100-kyr cycle, while the spectrum of the limestone thickness shows higher powers in the band on the 100-kyr eccentricity. The filter outputs of the whole eccentricity band of the marl thickness and marl-limestone couplet thickness are clearly dominated by the 405-kyr band, in phase with the variations in sedimentation rate calculated from the orbital tuning of the MS series and in phase with the kaolinite/illite, smectite and chlorite ratios (Fig. 4). In contrast, the filter output of the whole eccentricity in the limestone bed thicknesses shows a dominance of the 100-kyr eccentricity, but the phase relationship between this filter output and the other filter outputs changes throughout the whole time series, showing sometimes in phase (e13 and e14, Fig. 4), sometimes in anti-phase (e4, e7, e8, Fig. 4), or dephased. Therefore, the carbonate flux is not necessarily in anti-phase with the detrital flux. Such a change in phasing was also observed in the Valanginian of the Vocontian Basin (Pittet, 2006). At timescales of the eccentricity cycles, the sedimentation rates are controlled mainly by the detrital fluxes, themselves controlled by cyclic changes of levels of continental weathering and runoff. The carbonate flux controls the expression of the marl-limestone alternations at higher frequencies (100-kyr and higher).

4. BERSEK QUARRY

Gamma Ray Spectrometry (GRS), MS and bulk carbonate $\delta^{13}C$ ($\delta^{13}C_{carb}$) have been measured in the Bersek Marl Formation in the type locality of Bersek (Gerecse Hills) (Bajnai et al., 2017, Fig. 7). The lithology of the 31.2-m studied section evolves from a carbonate-dominated to marl-dominated alternations in the Purple Marl Formation. $\delta^{13}C_{carb}$ have been measured throughout the entire interval studied every 10 cm from 0 to 16.2 m to detect the Milankovitch cycles in this series, and then every 20 cm in order to observe the trend of the series and to correlate to other Tethyan sections. The $\delta^{13}C_{carb}$ series has a trend to stable values around

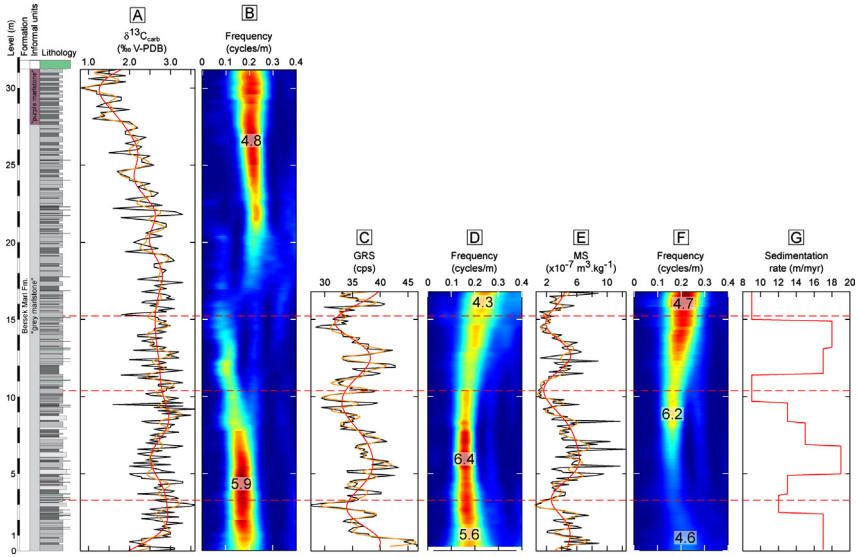

Figure 7 $\delta^{13}C_{carb}$, gamma-ray spectrometry (GRS) and magnetic susceptibility (MS) signals from the Bersek Quarry section together with evolutive spectral analyses and sedimentation rates. The *red* and the *orange curves* respectively represent the Taner low-pass filters of the 405-kyr and the whole eccentricity cycles. (A) $\delta^{13}C$ measured on bulk carbonate. (B) Spectrogram performed on 15-m width windows on the $\delta^{13}C$ signal. Periods are labeled in meters. (C) GRS signal. (D) Spectrogram performed on 15-m width windows on the MS signal. Periods are labeled in meters. (E) MS signal. (F) Spectrogram performed on 15-m width windows on the MS signal. Periods are labeled in meters. (G) Sedimentation rates calculated from the orbital calibration performed on the 100-kyr cycle on the MS signal (see Bajnai et al., 2017). The cut-off frequencies of the Taner low-pass filters are as follows: $\delta^{13}C_{carb}$: red curve: 0.3185 - cycles/m, orange curve: 1.1465 cycles/m; GRS: red curve: 0.3614 cycles/m, orange curve: 1.3855 cycles/m; MS: red curve: 0.3550 cycles/m, orange curve: 1.3018 cycles/m. The roll-off rate of all filters is set at 10^{36}.

2.7‰ (V-PDB) from 0 to 19.2 m, and then progressively decreases to mean values around 1.4‰ at the top of the studied section, in the Purple Marl Formation. The MS and GRS have been measured every 10 cm and 20 cm respectively with the aim to detect the orbital forcing in these marl–limestone alternations on the lowermost 16 m of the series. Both series show an obvious cyclic trend of 5 to 7 m in phase. The GRS signal depends on the gamma emission from the decay of Potassium 40 (^{40}K), Uranium 238 (^{238}U) and Thorium 232 (^{232}Th). These three radioactive elements are abundant in the continental crust (Serra, 1979). Erosion and chemical alteration during the pedogenesis phase concentrate K and Th in the clay

minerals while U is concentrated in clay minerals and in organic matter (Quirein et al., 1982; Schmoker, 1981). In organic-poor sediments, high GRS values indicate higher content in clay in the sediment. MS in phase with GRS also indicates high clay content in the sediment.

The spectra of these three series are calculated with the MTM using three 2π-tapers with confidence levels calculated with the Mann and Lees (1996) method modified in Meyers (2014). The spectra were generated after detrending the series as described in Bajnai et al. (2017). Evolutive spectral analyses were performed using the Time-Frequency Weighted Fast Fourier Transform (T-F WFFT, Martinez et al., 2015) on window width of 15 m to detect the low frequencies. The result of this spectral analysis is a 3-dimension spectrum, namely spectrogram, in which the high powers are shown in red colors while the spectral background is in blue colors (Fig. 7).

The 2π-MTM spectra show that the 405-kyr eccentricity cycle is expressed by the spectral peak at 5 m in all proxies (Fig. 8), the 100-kyr eccentricity by a band of periods ranging from 2.0 m to 0.8 m, the obliquity by the band of frequencies ranging from 0.8 to 0.44 m and the precession by the band of frequencies ranging from 0.32 to 0.21 m (Bajnai et al., 2017). In the low frequencies, the spectra of the MS and the GRS signals show a dominant peak in the 405-kyr band, which overwhelms the other bands (Fig. 8), while in the spectrum of the $\delta^{13}C_{carb}$, the 405-kyr band has a much lower amplitude and remains in the same level of the other bands. The high redness level of the spectrum of the GRS signal is due to the fact the GR probe receives the gamma signal over a radius of 20—30 cm, which smooths the high frequencies like a low-pass filter. The MS signal was measured in laboratory from discrete samples collected in the field and is thus not subject to this type of bias. The strong amplitude of the 405-kyr band thus reflects the strong response of lithological changes to this cycle. This strong impact of the 405-kyr cycle on the lithology is also observed in the sedimentation rates. Once the series is calibrated to the 100-kyr cycles observed in the MS signal (Fig. 7), the sedimentation rate shows an obvious cyclicity which follows the filters of the 405-kyr band in the MS and the GRS signals (Fig. 7). The higher the sedimentation rate is, the higher are the MS and the GRS values. As both signals carry a detrital signal, it implies that higher sedimentation rate occur when the detrital supply increases during more humid periods (Bajnai et al., 2017).

In the basal 10 m of the series, the $\delta^{13}C_{carb}$ shows an inverse correlation with MS and GRS at the scale of the 405-kyr cycle (Fig. 7). This inverse correlation stops around 10 m as the amplitude of the 405-kyr in the

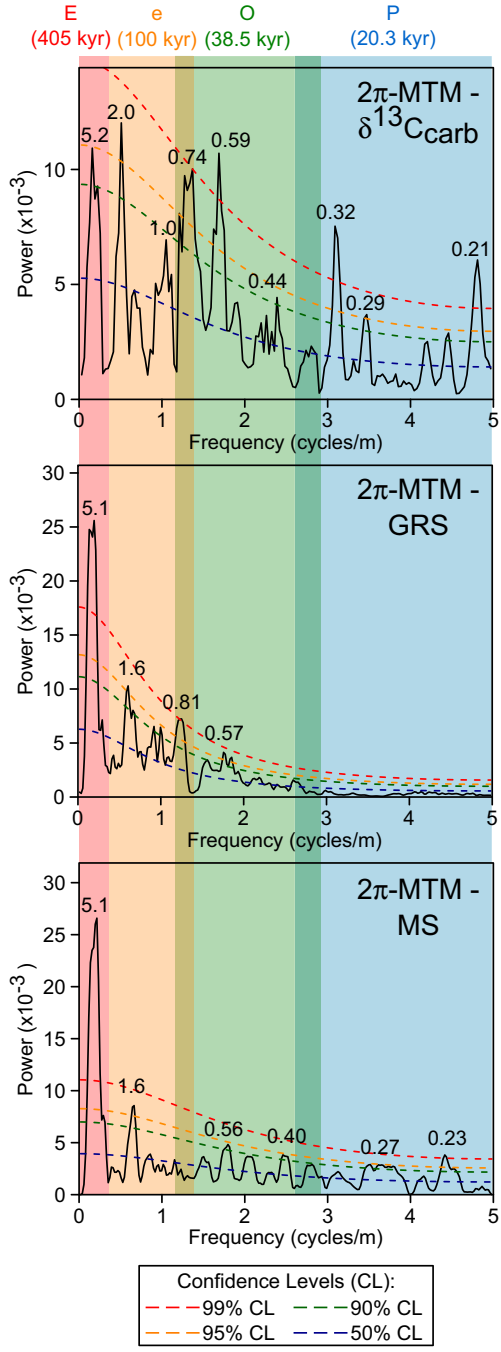

Figure 8 2π-MTM spectra of the $\delta^{13}C_{carb}$, GRS and the MS.

$\delta^{13}C_{carb}$ decreases. At 15 m, the filter output of 405-kyr cycle in the $\delta^{13}C_{carb}$ even shows a minimum in phase with the filter ouputs of the 405-kyr cycle of the the MS and GRS signals (Fig. 7). Thus, from 10 to 15 m, the filter output of the 405-kyr cycle in the $\delta^{13}C_{carb}$ evolves from an anti-phase to an in-phase relationship with the filter outputs of the 405-kyr cycle in the MS and GRS series. This interval from 10 to 15 m, where changes the phasing between the $\delta^{13}C_{carb}$ and the MS, also corresponds to a loss of amplitude and a node in the power spectrogram of the $\delta^{13}C_{carb}$ signal. Ultimately, the 405-kyr band loses its dominant power on the other cycles of the Milankovitch band in the spectrum of the $\delta^{13}C_{carb}$ series (Fig. 8). In hemipelagic areas, the $\delta^{13}C$ measured on bulk carbonate is a versatile proxy, because of the various sources of carbonate, such as export of photozoan or heterozoan carbonate platforms, in-situ pelagic carbonate productivity, in addition to dissolved bicarbonate being potentially influenced by the export of organic matter from the continent (Föllmi et al., 2006). All these sources have different $\delta^{13}C$ values and have different response times to the orbital forcing as they behave differently to humid or arid conditions. In the Western Transdanubian Range, important pelagic carbonate productivity took place from the Tithonian to the late Valanginian, while from the Barremian to the Albian, an important Urgonian-type carbonate platform developed northward of the Gerecse Hills, thus influencing carbonate deposition in the basin (Csaszar and Argyelan, 1994). The Bersek Marl and the Purple Marl Formations may represent a time of transition between various modes of carbonate input to the basin, which explains this change of phasing of the 405-kyr eccentricity in the $\delta^{13}C$ and its much lower amplitude than in the MS and the GRS signals. Such a phase shift triggered by change in carbonate input mode was notably observed in the Early Toarcian in Morocco (Ait-Itto et al., 2018) and resulted in a distortion of the expression of the orbital forcing on the $\delta^{13}C_{carb}$. Thus, much attention must be paid when calibrating time series with the $\delta^{13}C_{carb}$ in mixed carbonate-siliciclastic environments.

5. COMPOSITE VERGOL-MORÉNAS AND LA CHARCE-POMMEROL

GRS measurements have been carried out in the Vergol-Morénas and La Charce-Pommerol sections every 20 cm from the Early Valanginian to the Late Hauterivian (Fig. 9A; Martinez et al., 2013, 2015). The GRS signal increases form the Early to the Late Valanginian and from the early to the

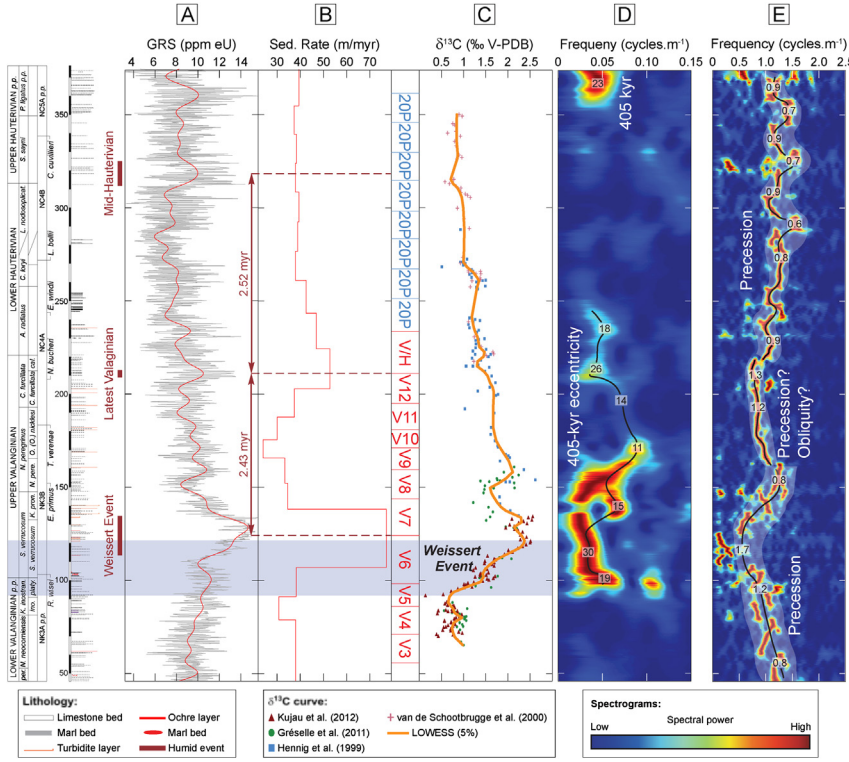

Figure 9 Gamma-ray spectrometry, spectral analyses and sedimentation rates of the composite Vocontian Basin series. (A) Gamma ray spectrometry curve (in gray), with the Taner low-pass filter of the (2.4-myr + 405-kyr) eccentricity band (in red). The Taner low-pass filter is performed on the GRS signal with a cut-off frequency of 0.1168 cycles/m. (B) Sedimentation rate calculated from the orbital calibration. (C) compilation of $\delta^{13}C_{carb}$ measured in the Vergol-Morénas, La Charce and Angles sections (data from Hennig et al., 1999; van de Schootbrugge et al., 2000; Gréselle et al., 2011; Kujau et al., 2012). The *orange curve* represents the Locally Weighted Scatterplot Smoothing (LOWESS; Cleveland, 1979) performed over 5% of the $\delta^{13}C$ data. (D) Spectrograms performed on 40-m width windows on the GRS signal. (E) Spectrograms performed on 15-m width windows on the GRS signal. Periods are labeled in meters.

Late Hauterivian, in two intervals where the marl-limestone alternations enrich in clay. Conversely, the GRS signal decreases from the Late Valanginian to the Early Hauterivian while the alternations become more carbonate-rich. The GRS signal thus follows the lithology and increases with the clay content. The spectral analyses were performed on the GRS signal (Martinez et al., 2013, 2015) using the T-F WFFT evolutive spectrogram (Martinez et al., 2015) on window width of 40 m to detect the low

frequencies (Fig. 9D) and a window width of 10 m to follow the evolution of the high frequencies (Fig. 9E).

The spectrograms show cycles from 10 to 30 m corresponding to the 405-kyr eccentricity and cycles from 0.7 to 1.7 m corresponding to the precession, except from 160 to 220 m, where it may reflect the obliquity. The series is calibrated in the Valanginian with the 405-kyr cycle, well expressed in this interval (Martinez et al., 2013; see also Fig. 1A). From the Radiatus Zone in the Hauterivian to the top of the series, the 405-kyr cycle is much less well expressed and I chose instead to calibrate the series on the precession, whose amplitude is much higher as shown on the evolutive spectrogram (Fig. 9E; see also Fig. 1). The sedimentation rate was calculated over two minima of the 405-kyr cycles until the top of cycle V/H (Fig. 9), and over 20 precession cycles, which represents a duration of 406 kyr, assuming a mean duration of the precession of 20.3 kyr during the Hauterivian (Waltham, 2015). This choice of calibration, in anti-phase with the "V" cycles of Martinez et al. (2013), makes it easier to compare the maxima of sedimentation rate to the maxima of the GRS signal. The sedimentation rate shows two maxima during the second half of the Weissert Event (cycles V6-V7) and at the Valanginian-Hauterivian boundary (cycles V12-V/H). Lower frequencies of the 405-kyr and the precession cycles are also observed in these intervals, confirming the increase in the sedimentation rate (Fig. 9). These two periods of high sedimentation rate coincide with higher GRS values, so that, once again, higher sedimentation rates correspond to higher detrital input. This relationship is also observed at the scale of the long-term trend: the maximum of sedimentation is observed during the second half of the Weissert Event, where the series reaches the maximum content in clay (Giraud et al., 1995). Then, the sedimentation rate decreases while the section becomes more carbonated. In the Late Hauterivian, the sedimentation rate remains stable while the GRS values increase. This interval is marked by a drowning event which decreases the neritic carbonate productivity (Föllmi et al., 2006). The thickness of the limestone beds decreases while the thickness of the marlstone beds increases, stabilizing the sedimentation rate. Such a stabilization of the sedimentation is not observed during the drowning phase of the mid-Valanginian Weissert Event (Fig. 9). During the mid-Valanginien Event, the kaolinite content of the clay fraction reaches 40% (Charbonnier et al., 2016; Fesnau, 2008), while it only reaches 10% in the early Late Hauterivian (Godet et al., 2008). During the Weissert Event, the acceleration of the hydrological cycle, likely a consequence of widespread volcanism from the Paraná-Etendeka large igneous province

(Charbonnier et al., 2017; Martinez et al., 2015), triggered large increase in the levels of continental weathering and detrital export to the basin, which explains why the sedimentation rate increase during the mid-Valanginian despite the loss in carbonate export.

The GRS values are maximal during the mid-Valanginian Event (cycles V6-V7), at the end of the Valanginian (cycles V12-V/H) and in the early Late Hauterivian (Sayni Zone) (Fig. 9). These maximums in GRS are separated by 2.4 to 2.5 myr, suggesting that the 2.4-myr eccentricity cycle controlled the recurrence of these peaks in GR. The 2.4-myr cycle also controlled the variation in the sedimentation rate during the Valanginian, as two of the maxima in the GRS signal also coincide with higher sedimentation rates (Fig. 9). Pollen contents and clay mineralogy also show higher humidity levels during the mid-Valanginian and the latest Valanginian paced by the 2.4-myr cycle (Charbonnier et al., 2016; Kujau et al., 2013). The 2.4-myr eccentricity cycle thus paced higher humidity levels, marked by higher content in spore, kaolinite and clay in the sediment. The pacing of the 2.4-myr cycle continues to the Hauterivian, as it paces the occurrence of the mid-Hauterivian humid peak. Thus the 2.4-myr cycle appears to be the pacemaker of the occurrence of transient humid events, at the Berraisian-Valanginian boundary, in the mid-Valanginian, in the latest Valanginian and in the mid-Hauterivian.

6. ORBITAL IMPACT ON DETRITAL INPUT: SIMULATIONS

6.1 Effect of Memory in Erosion Processes

Several lessons can be obtained from our three case studies. In the Río Argos section, lithological proxies have shown a dominance of the 100-kyr cycle while the detrital proxies have shown a dominance of the 405-kyr cycle (Figs. 4 and 6). In the Bersek Quarry, the MS and the GR have shown a dominance of the 405-kyr cycle while the $\delta^{13}C_{carb}$ has shown a suppression of the amplitude of the cycle due to a phase shift with the MS and the GRS (Figs. 7 and 8). In the Vocontian Basin, the detrital input has shown a cyclicity linked to the 405-kyr and to the 2.4-myr cycle (Fig. 9). Therefore, these three examples show that the detrital input is controlled by the eccentricity cycles with a much higher amplitude than the carbonate export to the basin.

It can be surprising to see such a strong influence of the eccentricity cycles in the detrital input despite its very weak power and the predominance of the precession cycles in the power spectrum of the insolation series at low latitudes (Berger and Loutre, 1994). The dominance of the eccentricity cycles in the detrital supply to the basin implies non-linear mechanisms. Pedogenesis, erosion and sediment transport are strong potential sources of transfer of power from the high to the low frequencies (Armitage et al., 2013). Notably, pedogenesis processes are the consequence of the state of the environment at a time *t*, but also the state of the soil at time *t-n* (Targulian and Krasilnikov, 2007). Changes in soil, erosion and sediment transport are thus progressive, time averaging, and take into account the state of the environment at previous times. As soil development may take up to 10^6 yr for the most developed soils (Lin, 2011), continental weathering and erosion may act as a moving average over 10^4 to 10^6 yr.

Fig. 10 shows the insolation solution at 25°N from 0.5 to 3.5 Ma (Fig. 10A), with the spectrum of this insolation series calculated over the last 50 myr (Fig. 10B). The power spectrum is dominated by the record of the precession cycles, the other cycles being hardly observable. I applied to the insolation signal a Gaussian-weighted Moving Average (GMA) oriented to the past to simulate the memory effect of the erosion processes to the insolation (Figs. 10C, F, and I). Applying a GMA over 75 kyr disrupts the amplitude modulation pattern on the precession cycles, leading to a power transfer to the eccentricity cycles (Figs. 10C–E). With a GMA over 75 kyr, the 405-kyr cycle has an amplitude as high as the precession cycles, while the amplitude of the 100-kyr cycle is clearly visible in the spectrum (Fig. 10D–E). With a GMA over 500 kyr, the 405-kyr cycle clearly dominates the power spectrum (Fig. 10G and H), while the residual insolation forms clear sequences of ~400 kyr (Fig. 10F). In addition, a sequence of ~2 myr can be observed in the insolation series while a peak at 2.4 myr is visible in the spectrum. With a GMA over 1 myr (maximum of memory effect if I only take into account pedogenetic effects), a clear sequence of ~2 myr dominates the insolation series and the spectrum, while the amplitude of the precession cycles is very weak in comparison to the eccentricity (Figs. 10I–K).

Longer memory effects tend to favor the expression of the 405-kyr and the 2.4-myr eccentricity cycles. As more humid climates led to more detrital inputs to the basin and to more profound pedogenetic processes, they also led to long memory effects in clayey formations which favored a much stronger expression of the 405-kyr and the 2.4-myr eccentricity cycles

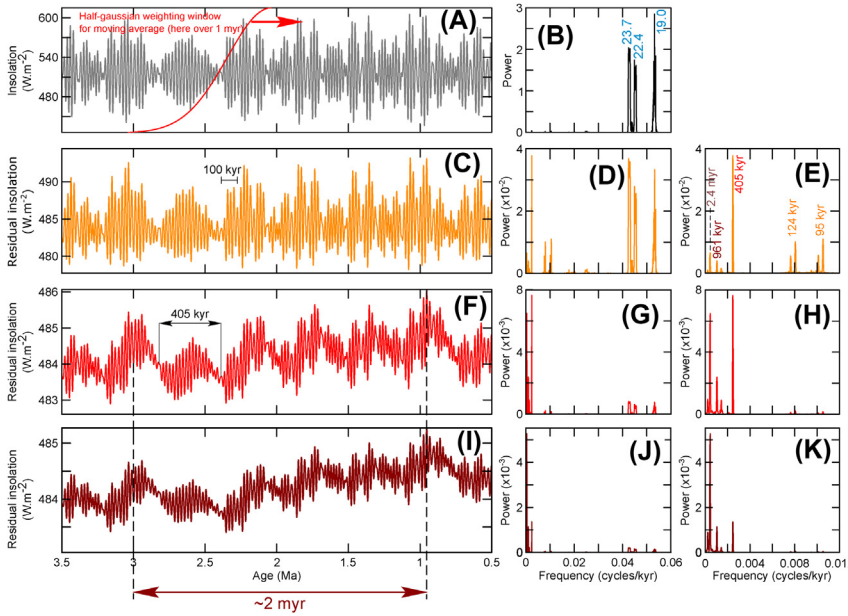

Figure 10 Tests of memory effects applying Gaussian weigthed Moving Averages (GMA) on the insolation series on 21st June at 25°N. (A) Insolation at 25°N on June 21st. The *red curve* represents the shape of the gaussian-distributed weigthed coefficients used to apply the moving averages. (C), (F) and (I) Residual insolation after applying GMAs, respectively at 75 kyr (panel C.), 500 kyr (panel F.) and 1 myr (panel I.). (B), (D), (G) and (J) Spectra of the insolation of residual insolation series shown over the full Milankovitch band. (E), (H), (K) Details of the spectra of the residual insolation series on the eccentricity band.

compared to carbonate-dominated formations. This interpretation can explain why striking bundles of 405 kyr are observed in the Upper Valanginian of the Vocontian Basin but not in the Early Hauterivian (see Figs. 1C—D). Other such examples can be found in the Aptian '*Marnes Bleues*' Formation (Vocontian basin; Ghirardi et al., 2014) or in the Late Jurassic '*Terres Noires*' Formation (Vocontian basin; Boulila et al., 2010).

6.2 Effect of Phase Shifting on the Insolation Forcing

It is noteworthy that in the previous simulations, the 405-kyr eccentricity cycle has always a stronger amplitude than the 100-kyr eccentricity cycle, while in sedimentary series, stronger amplitudes can be observed in the 100-kyr band (Figs. 6 and 8). Higher amplitudes in the 100-kyr band are notably observed at Río Argos in the lithological proxies, while the proxies

of detrital input preserve stronger amplitudes in the 405-kyr band (Fig. 6). In the Bersek Quarry, the $\delta^{13}C_{carb}$ shows higher amplitudes in the 100-kyr band than the MS and the GRS, as the $\delta^{13}C_{carb}$ changes its phasing to the MS and the GRS (Figs. 7 and 8). The response of the carbonate producers to eustatism and climate is still a matter of debate and the variations of the carbonate exports or $\delta^{13}C_{carb}$ to insolation changes can have opposite trends depending on the carbonate producers or the morphology of the platforms surrounding the basin (Föllmi et al., 2006; Pittet and Strasser, 1998; Pittet, 2006; Schlager et al., 1994). The flooding of a carbonate platform during a transgression increases the neritic carbonate production and the export of this production to the basin (Schlager et al., 1994). On a ramp morphology, changes in the sea level moves the neritic carbonate production farther from or closer to the basin but does not change the amount of neritic carbonate produced (Pittet, 2006), leading for instance to less export of neritic carbonate to the basin at times of sea-level highs. This change in the response of the carbonate productivity to an external forcing triggers a change of phasing between carbonate and detrital exports, which notably explains the change in phasing between the thickness of the limestone beds and the marl beds in the Río Argos section (Fig. 4). The phasing between $\delta^{13}C$ and the orbital forcing can also change depending on the source of the carbonate (Föllmi et al., 2006). Photozoan carbonate-platforms, usually aragonitic producers, have higher $\delta^{13}C$ values than heterozoan calcitic platforms. The $\delta^{13}C$ values of hemipelagic carbonates thus reflect the isotopic composition of the carbonates produced in the neritic environments. As photozoan and heterozoan environments develop in different climatic settings, the change in neritic carbonate producer can change the phasing between the $\delta^{13}C_{carb}$ and the orbital forcing. This possibly explains the change of phasing between the $\delta^{13}C_{carb}$ and the MS and GRS in the Bersek Quarry (Fig. 7). It may also explain the change of phasing between the thicknesses of the limestone and the marl beds in the Río Argos section (Fig. 4).

I tested the impact of the change in phasing in the insolation series (Fig. 11). For this, I selected the interval of the residual insolation after applying a GMA over 75 kyr (Fig. 11A) from 2.4 to 0.9 Ma. The interval covers 1.5 myr as in the Río Argos of Bersek Quarry sections and avoids specific intervals of minimums of the 2.4-myr cycle, where the 100-kyr cycle reaches a minimum in amplitude. I selected an interval covering 0.4 myr from 2 to 1.6 Ma in which I inversed the residual insolation to simulate the change of phasing of the proxy to the insolation (labeled as

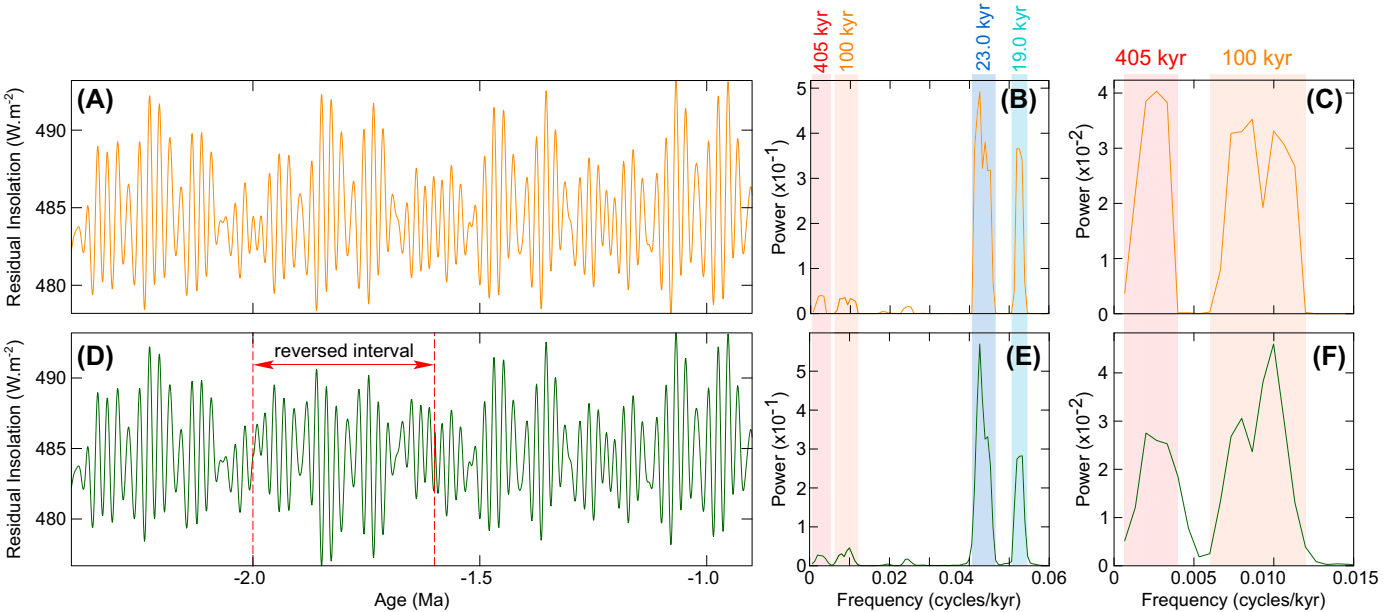

Figure 11 Impact of changing the phasing of the insolation on the spectral analyses in the Milankovitch band. (A) Residual insolation series after applying a Gaussian weighted Moving Average over 75 kyr (same as in Fig. 10C). (B) Spectrum of the residual insolation shown in panel (A). (C) Focus of the spectrum in panel (B) on the eccentricity band. (D) Residual insolation series after changing the phasing of the curve in panel (A) at 2 Ma and 1.6 Ma. The *dash red lines* indicate where the change of phasing have been made (called "reversed interval"). (E) Spectrum of the residual insolation shown in panel (D). (F) Focus of the spectrum in panel (E) on the eccentricity band.

"reversed interval" in Fig. 11D). The interval from 2 to 1.6 Ma is thus in anti-phase with the residual insolation while the rest of the series remains in phase. Compared to the spectrum after applying a GMA over 75 kyr, the spectrum of the series after applying phase changes displays higher amplitudes in the 100-kyr band than in the 405-kyr band (Figs. 11E and F). However, the precession cycle remains dominant in the power spectrum (Fig. 11E). Our experiment thus shows that the amplitude of the 100-kyr cycle can be significantly enhanced with respect to the 405-kyr cycle by changing in-phase relationship between a proxy and the insolation.

Other phenomena must apply to decrease the amplitude of the precession cycles and make the 100-kyr eccentricity the dominant cycle in the power spectrum. Orbital cycles impact the detrital input to the basin, which impact in turn the sedimentation rates (Figs. 4, 7 and 9). I imposed cyclical variations of the sedimentation rates on the residual insolation series after applying the phase shifts (Fig. 12A). The experiment thus simulates the same cyclical variations of the sedimentation rates as observed in Río Argos. The average sedimentation rate is 2.85 cm/kyr. It varies with a mean amplitude of 0.85 cm/kyr with a period of 405 kyr. The resulting spectrum (Fig. 12A) still shows a dominant power in the precession band, so the variations in the sedimentation rates cannot explain alone the dominance of the 100-kyr cycle.

The bioturbation can decrease the amplitude of the high frequencies in the power spectrum below a sedimentation rate of 3 cm/kyr (Pisias, 1983). I simulated the impact of bioturbation in a sedimentary series by applying a simple moving average over 19 kyr on the residual insolation series after applying changing in phasing (Fig. 12B). As a result, the power of the precession decreases and the band of the 100-kyr cycle becomes dominant in the power spectrum. Bioturbation processes alone are thus enough to explain the decrease in power of the precession band, allowing the 100-kyr eccentricity to become dominant in case of a weak effect memory from erosional processes and phase shifts in the low frequencies. Applying bioturbation processes over one precession period after having applied variations in the sedimentation rates on the residual insolation series does not completely erase the power of the precession cycles, though. However, it is noteworthy that only the precession cycle at 23 kyr (namely P1) is observed (Fig. 12C), the power of the 19-kyr precession cycle (P2) being completely flattened out.

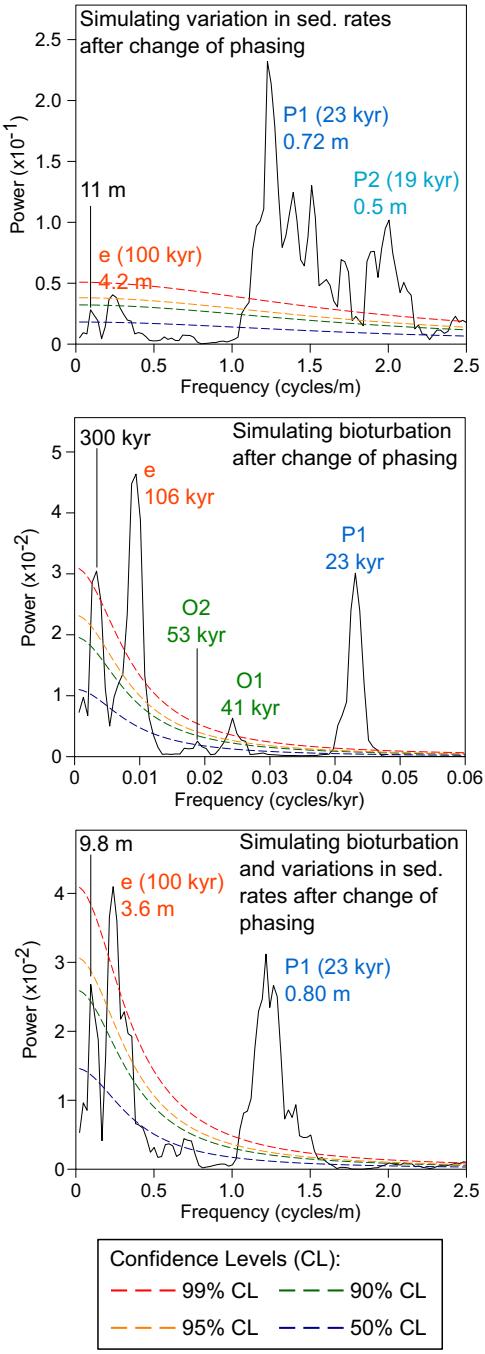

Figure 12 2π-MTM spectra of the residual insolation after changing the phasing (curve in Fig. 11D) and applying variations in sedimentation rates and bioturbation. The confidence levels (CL) are calculated using the Mann and Lees (1996) method modified in Meyers (2014).

7. CONCLUSIONS

In this paper, three case-studies were reviewed to explore the potential mechanisms of transfer of power from the precession to the eccentricity band in Early Cretaceous hemipelagic marl-limestone alternations of the Tethyan area. Higher sedimentation rates are observed in the most clayey intervals of the series showing the highest contents in kaolinite. More carbonated intervals show various phasing with the detrital input and thus do not preserve the lowest frequencies. More humid climate leads to higher detrital input to the basin and higher sedimentation rates in hemipelagic marl-limestone alternations. Memory effects of the erosional and pedogenetic processes are proposed as sedimentary mechanisms responsible for the transfer of power from the precession to the eccentricity band. Higher memory effects due to evolved pedogenetic processes during more humid climate conditions reinforce the 405-kyr and the 2.4-myr eccentricity cycles and can explain their high amplitudes in the sedimentary series in contrast to their weak amplitudes in the insolation series. Conversely, weak memory effects during more arid phases associated to changes in the phasing between orbital cycles and the carbonate production can decrease the amplitude of the long eccentricity cycles and explain the dominance of the 100-kyr cycle in the eccentricity band. Lower sedimentation rates during these intervals can favor the impact of the bioturbation on the sedimentation, which decreases the amplitude of the precession cycles and reinforces the dominance of the 100-kyr eccentricity cycles in the power spectrum of the sedimentary series.

ACKNOWLEDGMENTS

This is a contribution from Team PALEO2D from Geosciences Rennes. I acknowledge anonymous reviewers for their comments. I warmly acknowledge Nicolas Thibault for his positive feedback and his suggestions to improve the quality of the manuscript.

REFERENCES

Ait-Itto, F.-Z., Martinez, M., Price, G.D., Ait Addi, A., 2018. Synchronization of the astronomical time scales in the Early Toarcian: a link between anoxia, carbon-cycle perturbation, mass extinction and volcanism. Earth Planet Sci. Lett. 493, 1–11.

Armitage, J.J., Jones, T.D., Duller, R.A., Whittaker, A.C., Allen, P.A., 2013. Temporal buffering of climate-driven sediment flux cycles by transient catchment response. Earth Planet Sci. Lett. 369-370, 200–210.

Bajnai, D., Pálfy, J., Martinez, M., Price, G.D., Nyerges, A., Főzy, I., 2017. Multi-proxy record of orbital-scale changes in climate and sedimentation during the Weissert event in the Valanginian Bersek Marl formation (Gerecse Mts., Hungary). Cretac. Res. 75, 45–60.

Baudin, F., Riquier, L., 2014. The late Hauterivian Faraoni 'oceanic anoxic event': an update. B. Soc. Geol. Fr. 185, 359–377.
Berger, A., Loutre, M.-F., 1994. Precession, eccentricity, obliquity, insolation and paleoclimates. In: Duplessy, J.-C., Spyridakis, M.-T. (Eds.), Long-term Climatic Variations, NATO ASI Series, vol. I 22. Springer-Verlag, Berlin, pp. 107–151.
Blanc, E., 1996. Transect plate-forme - bassin dans les séries carbonatées du Berriasien supérieur et du Valanginien inférieur (domaines jurassien et nord-vocontien). Geol. Alp., Mémoire H.S. 25 (Grenoble, France).
Boulila, S., Galbrun, B., Hinnov, L.A., Collin, P.-Y., Ogg, J.G., Fortwengler, D., Marchand, D., 2010. Milankovitch and sub-Milankovitch forcing of the Oxfordian (Late Jurassic) Terres Noires formation (SE France) and global implications. Basin Res. 22, 717–732.
Bulot, L.G., Thieuloy, J.-P., Blanc, E., Klein, J., 1993. Le cadre stratigraphique du Valanginien supérieur et de l'Hauterivien du Sud-Est de la France: définition des biochronozones et caractérisation de nouveaux biohorizons. Geol. Alp. 1992, 13–56.
Cleveland, W.S., 1979. Robust locally weighted regression and smoothing scatterplots. J. Am. Stat. Assoc. 74, 829–836.
Cotillon, P., 1971. Le Crétacé inférieur de l'Arc subalpin de Castellane entre l'Asse et le Var : stratigraphie et sédimentologie, Mémoires du B.R.G.M. 68. Editions B.R.G.M., Paris, France.
Cotillon, P., 1987. Bed-scale cyclicity of pelagic Cretaceous successions as a result of world-wide control. Mar. Geol. 78, 109–123.
Cotillon, P., Ferry, S., Gaillard, C., Jautée, E., Latreille, G., Rio, M., 1980. Fluctuation des paramètres du milieu marin dans le domaine vocontien (France Sud-Est) au Crétacé inférieur : mise en évidence par l'étude des formations marno-calcaires alternantes. B. Soc. Geol. Fr., t. XXII (5), 735–744.
Chamley, H., 1989. Clay Sedimentology. Springer-Verlag, Berlin, Germany.
Charbonnier, G., Duchamp-Alphonse, S., Adatte, T., Föllmi, K.B., Spangenberg, J.E., Gardin, S., Galbrun, B., Colin, C., 2016. Eccentricity pacedmonsoon-like systemalong the northwestern Tethyan margin during the Valanginian (Early Cretaceous): new insights from detrital and nutrient fluxes into the Vocontian Basin (SE France). Palaeogr. Palaeocl. 443, 145–155.
Charbonnier, G., Morales, C., Duchamp-Alphonse, S., Westermann, S., Adatte, T., Föllmi, K.B., 2017. Mercury enrichment indicates volcanic triggering of Valanginian environmental change. Sci. Rep. 7, 40808.
Colombié, C., Strasser, A., 2003. Depositional sequences in the Kimmeridgian of the Vocontian Basin (France) controlled by carbonate export from shallow-water platforms. Geobios 675–683.
Császár, G., Árgyelán, T., 1994. Stratigraphic and micromineralogic investigations on Cretaceous formations of the Gerecse Mountains, hungary and their palaeogeographic implications. Cretac. Res. 15, 417–434.
Csontos, L., Vörös, A., 2004. Mesozoic plate reconstruction of the Carpathian region. Palaeogr. Palaeocl. 210, 1–56.
Darmedru, C., Cotillon, P., Rio, M., 1982. Rythmes climatiques et biologiques en milieu marin pélagique : leur relation dans les dépôts crétacés alternants du Bassin Vocontien (S.E. France). B. Soc. Geol. Fr., Série XXIV 7, 627–640.
Deconinck, J.-F., Chamley, H., 1983. Héritage et diagenèse des minéraux argileux dans les alternances marno-calcaires du Crétacé inférieur du domaine subalpin. C. R. Acad. Sci. II 297, 589–594.
Deconinck, J.-F., Debrabant, P., 1985. Diagenèse des argiles dans le domaine subalpin : rôles respectifs de la lithologie, de l'enfouissement et de la surcharge tectonique. Rev. Geol. Dyn. Geogr. 26, 321–330.

Dercourt, J., Ricou, L.E., Vrielynck, B., 1993. Atlas Tethys Paleoenvironmental Maps. Gauthier-Villars, Paris, France.
De Wever, P., 1987. Radiolarites rubanées et variations de l'orbite terrestre. B. Soc. Geol. Fr., Série VIII 3, 957–960.
Fesnau, C., 2008. Enregistrement des changements climatiques dans le domaine téthysien au Valanginien (PhD Thesis). Université de Bourgogne, UMR Biogéosciences, Dijon, France.
Fodor, L., Főzy, I., 2013. Late middle Jurassic to earliest Cretaceous evolution of basin geometry of the Gerecse Mountains. In: Főzy, I. (Ed.), Late Jurassic–early Cretaceous Fauna, Biostratigraphy, Facies and Deformation History of the Carbonate Formations in the Gerecse and Pilis Mountains (Transdanubian Range, Hungary). Institute of Geosciences, University of Szeged, GeoLitera Publishing House, Szeged, pp. 117–136.
Fodor, L., Sztanó, O., Köver, S., 2013. Mesozoic deformation of the northern Transdanubian range (Gerecse and Vértes Hills). Acta Mineral. Petrogr., Field Guide Series 31, 1–34.
Fogarasi, A., 2001. Lower Cretaceous Calcareous Nannoplankton Stratigraphy of the Transdanubian Range. PhD Thesis. Eötvös University, Department of General and Historical Geology, Budapest, Hungary.
Föllmi, K.B., Godet, A., Bodin, S., Linder, P., 2006. Interactions between environmental change and shallow water carbonate buildup along the northern Tethyan margin and their impact on the Early Cretaceous carbon isotope record. Paleoceanography 21, PA4211.
Föllmi, K.B., 2012. Early Cretaceous life, climate and anoxia. Cretac. Res. 35, 230–257.
Főzy, I., Janssen, N.M.M., 2009. Integrated lower Cretaceous biostratigraphy of the Bersek Quarry, Gerecse Mountains, Transdanubian range, Hungary. Cretac. Res. 30, 78–92.
Ghirardi, J., Deconinck, J.-F., Pellenard, P., Martinez, M., Bruneau, L., Amiotte-Suchet, P., Pucéat, E., 2014. Multi-proxy orbital chronology in the aftermath of the Aptian ocean Anoxic event 1a: Palaeoceanographic implications (Serre Chaitieu section, Vocontian basin, SE France). Newsl. Stratigr. 47, 247–262.
Gilbert, G.K., 1895. Sedimentary measurement of Cretaceous time. J. Geol. 3, 121–127.
Giraud, F., Beaufort, L., Cotillon, P., 1995. Periodicities of carbonate cycles in the Valanginian of the Vocontian Trough: a strong obliquity control. In: House, M.R., Gale, A.S. (Eds.), Orbital Forcing Timescales and Cyclostratigraphy, Geol. Soc. Sp. Publ., vol. 85, pp. 143–164. London.
Giraud, F., Reboulet, S., Deconinck, J.-F., Martinez, M., Carpentier, A., Bréziat, C., 2013. The Mid-Cenomanian event in Southeastern France: evidence from palaeontological and clay mineralogical data. Cretac. Res. 46, 43–58.
Godet, A., Bodin, S., Adatte, T., Föllmi, K.B., 2008. Platform-induced clay-mineral fractionation along a northern Tethyan basin-platform transect: implications for the interpretation of Early Cretaceous climate change (Late Hauterivian-Early Aptian). Cretac. Res. 29, 830–847.
Gréselle, B., Pittet, B., Mattioli, E., Joachimski, M., Barbarin, N., Riquier, L., Reboulet, S., Pucéat, E., 2011. The Valanginian isotope event: a complex suite of palaeoenvironmental perturbations. Palaeogr. Palaeocl. 306, 41–57.
Hennig, S., Weissert, H., Bulot, L., 1999. C-isotope stratigraphy, a calibration tool between ammonite and magnetostratigraphy: the Valanginian-Hauterivian transition. Geol. Carpath. 50, 91–96.
Herbert, T.D., 1994. Reading orbital signals distorted by sedimentation: models and examples. In: de Boer, P.L., Smith, D.G. (Eds.), Orbital Forcing and Cyclic Sequences, Sp. Publ. Int. Ass. Sediment, vol. 19, pp. 483–507. Oxford.
Hinnov, L.A., Park, J.J., 1999. Strategies for assessing early–middle (Pliensbachian–Aalenian) Jurassic cyclochronologies. Phil. Trans. R. Soc. A 357, 1831–1859.

Hoedemaeker, P.J., Leereveld, H., 1995. Biostratigraphy and sequence stratigraphy of the Berriasian-lowest Aptian (lower Cretaceous) of the Río Argos succession, Caravaca, SE Spain. Cretac. Res. 16, 195–230.
Hunt, C.P., Moskowitz, B.M., Banerjee, S.K., 1995. Magnetic properties of rocks and minerals. In: Ahrens, T.J. (Ed.), Rock Physics & Phase Relations, AGU Reference Shelf Series, vol. 3, pp. 189–204. Washington D.C.
Kujau, A., Heimhofer, U., Ostertag-Henning, C., Gréselle, B., Mutterlose, J., 2012. No evidence for anoxia during the Valanginian carbon isotope event—an organic-geochemical study from the Vocontian Basin, SE France. Global Planet. Change 92-93, 92–104.
Kujau, A., Heimhofer, U., Hochuli, P.A., Pauly, S., Morales, C., Adatte, T., Föllmi, K., Ploch, I., Mutterlose, J., 2013. Reconstructing Valanginian (Early Cretaceous) mid-latitude vegetation and climate dynamics based on spore-pollen assemblages. Rev. Palaeobot. Palynol. 197, 50–69.
Laurin, J., Meyers, S.R., Uličný, D., Jarvis, I., Sageman, B.B., 2015. Axial obliquity control on the greenhouse carbon budget through middle- to high-latitude reservoirs. Paleoceanography 30. https://doi.org/10.1002/2014PA002736.
Lemoine, M., Bas, T., Arnaud-Vanneau, A., Arnaud, H., Dumont, T., Gidon, M., Bourbon, M., de Graciansky, P.-C., Rudkiewicz, J.-L., Megard-Galli, J., Tricart, P., 1986. The continental margin of the Mesozoic Tethys in the western Alps. Mar. Petrol. Geol. 3, 179–199.
Lin, H., 2011. Three principles of soil change and pedogenesis in time and space. Soil Sci. Soc. Am. J. 75, 2049–2070.
Mann, M.E., Lees, J.M., 1996. Robust estimation of background noise and signal detection in climatic time series. Climatic Change 33, 409–445.
Martín-Algarra, A., Ruiz-Ortiz, P.A., Vera, J.A., 1992. Factors controlling Cretaceous turbidite deposition in the Betic Cordillera. Rev. Soc. Geol. Esp. 5, 53–80.
Martinez, M., Deconinck, J.-F., Pellenard, P., Reboulet, S., Riquier, L., 2013. Astrochronology of the Valanginian stage from reference sections (Vocontian basin, France) and palaeoenvironmental implications for the Weissert event. Palaeogr. Palaeocl. 376, 91–102.
Martinez, M., Deconinck, J.-F., Pellenard, P., Riquier, L., Company, M., Reboulet, S., Moiroud, M., 2015. Astrochronology of the Valanginian-Hauterivian stages (Early Cretaceous): chronological relationships between the Paraná-Etendeka large igneous province and the Weissert and the Faraoni events. Global Planet. Change 131, 158–173.
Martinez, M., Krencker, F.-N., Mattioli, E., Bodin, S., 2017. Orbital chronology of the Pliensbachian–Toarcian transition from the central high Atlas basin (Morocco). Newsl. Stratigr. 50, 47–69.
Martinez, M., Pellenard, P., Deconinck, J.-F., Monna, F., Riquier, L., Boulila, S., Moiroud, M., Company, M., 2012. An orbital floating time scale of the Hauterivian/Barremian GSSP from a magnetic susceptibility signal. Cretac. Res. 36, 106–115.
Meyers, S.R., 2014. Astrochron: An R Package for Astrochronology. Available at. https://cran.r-project.org/web/packages/astrochron/index.html.
Meyers, S.R., Sageman, B.B., 2004. Detection, quantification, and significance of hiatuses in pelagic and hemipelagic strata. Earth Planet Sci. Lett. 224, 55–72.
Moiroud, M., Martinez, M., Deconinck, J.-F., Monna, F., Pellenard, P., Riquier, L., Company, M., 2012. High-resolution clay mineralogy as a proxy for orbital tuning: example of the Hauterivian–Barremian transition in the Betic Cordillera (SE Spain). Sediment. Geol. 282, 336–346.
Mutterlose, J., Ruffell, A., 1999. Milankovitch-scale palaeoclimate changes in pale–dark bedding rhythms from the Early Cretaceous (Hauterivian and Barremian) of eastern England and northern Germany. Palaeogr. Palaeocl. 154, 133–160.

Ogg, J.G., Ogg, G.M., Gradstein, F.M., 2016. A Concise Geologic Time Scale 2016. Elsevier B.V., Amsterdam, The Netherlands.
Pisias, N.G., 1983. Geologic time series from deep-sea sediments: time scales and distortion by bioturbation. Mar. Geol. 51, 99–113.
Pittet, B., 2006. Les alternances marno-calcaires ou l'enregistrement de la dynamique de production et d'export des plates-formes carbonatées (Habilitation Thesis). Université Claude Bernard Lyon 1, UMR PaléoEnvironnements et PaléobioSphère, 79 pp.
Pittet, B., Mattioli, E., 2002. The carbonate signal and calcareous nannofossil distribution in an Upper Jurassic section (Balingen-Tieringen, Late Oxfordian, Southern Germany). Palaeogr. Palaeocl. 179, 71–96.
Pittet, B., Strasser, A., 1998. Depositional sequences in deep-shelf environments formed through carbonate-mud import from the shallow platform (Late Oxfordian, German Swabian Alb and eastern Swiss Jura). Eclogae geol. Helv. 91, 149–169.
Quirein, J.A., Gardner, J.S., Watson, J.T., 1982. Combined natural gamma-ray spectral litho-density measurements applied to clay mineral identification. AAPG Bull. 66, 1446.
Reboulet, S., Atrops, F., 1999. Comments and proposals about the Valanginian-Lower Hauterivian ammonite zonation of south-eastern France. Eclogae Geol. Helv. 92, 183–197.
Roux, M., Bourseau, J.-P., Bas, T., Dumont, T., de Graciansky, P.-C., Lemoine, M., Rudkiewicz, J.-L., 1988. Bathymetric evolution of the Tethyan margin in the western Alps (data from stalked crinoids): a reappraisal of eustatism problems during the Jurassic. B. Soc. Geol. Fr., tome 4 (4), 633–641.
Sauvage, L., Riquier, L., Thomazo, C., Baudin, F., Martinez, M., 2013. The late Hauterivian Faraoni "oceanic anoxic event" at Río Argos (southern Spain): an assessment on the level of oxygen depletion. Chem. Geol. 340, 77–90.
Schmoker, J.W., 1981. Determination of organic-matter content of Appalachian Devonian shales from gamma-ray logs. AAPG Bull. 65, 1285–1298.
Serra, O., 1979. Diagraphies différées. Bases de l'interprétation. Tome 1 : Acquisition des données diagraphiques. Bulletin du Centre de Recherche Exploration-Production Elf-Aquitaine, Pau, France.
Schlager, W., Reijmar, J.J.G., Droxler, A., 1994. Highstand shedding of carbonate platforms. J. Sediment. Res. B64, 270–281.
Stampfli, G.M., Borel, G.D., 2002. A plate tectonic model for the Paleozoic and Mesozoic constrained by dynamic plate boundaries and restored synthetic oceanic isochrons. Earth Planet Sci. Lett. 196, 17–33.
Taner, M.T., 2003. Attributes Revisited. Technical Publication, Rock Solid Images, Inc., Houston, TX. rocksolidimages.com/pdf/attrib_revisited.htm.
Targulian, V.O., Krasilnikov, P.V., 2007. Soil system and pedogenic processes: self-organization, time scales, and environmental significance. Catena 71, 373–381.
Thierstein, H.R., 1973. Lower Cretaceous Calcareous Nannofossil Biostratigraphy. In: Abhandlungen der Geologischen Bundensanstalt, vol. 29. Geologische Bundensanstalt, Vienna, Austria.
Thomson, D.J., 1982. Spectrum estimation and harmonic analysis. Proc. IEEE 70, 1055–1096.
Thomson, D.J., 1990. Quadratic-inverse spectrum estimates: applications to palaeoclimatology. Phil. Trans. R. Soc. A 332, 539–597.
van de Schootbrugge, B., Föllmi, K.B., Bulot, L.G., Burns, S.J., 2000. Paleoceanographic changes during the Early Cretaceous (Valanginian-Hauterivian): evidence from oxygen and carbon stable isotopes. Earth Planet Sci. Lett. 181, 15–31.
Vera, J.A., 2001. Evolution of the South Iberian continental margin. In: Ziegler, P.A., Cavazza, W., Robertson, A.H.F., Crasquin-Soleau, S. (Eds.), Peri-tethys Memoir 6: Peri-tethyan Rift/Wrench Basins and Passive Margins. Mémoires du Museum National d'Histoire Naturelle, Paris, pp. 109–143.

Waltham, D., 2015. Milankovitch period uncertainties and their impact on cyclostratigraphy. J. Sediment. Res. 85, 990–998.
Westphal, H., Hilgen, F., Munnecke, A., 2010. An assessment of the suitability of individual rhythmic carbonate successions for astrochronological application. Earth-Sci. Rev. 99, 19–30.
Wilpshaar, M., Leereveld, H., Visscher, H., 1997. Early Cretaceous sedimentary and tectonic development of the Dauphinois basin (SE France). Cretac. Res. 18, 457–468.